Zang *et al.*
*Protection and Control of Modern Power Systems* (2022) 7:23
https://doi.org/10.1186/s41601-022-00243-0

Protection and Control of Modern Power Systems

ORIGINAL RESEARCH Open Access

# A d-axis based current differential protection scheme for an active distribution network

Lindong Zang[1], Guibin Zou[1*], Chenghan Zhou[1], Maoran Zheng[2] and Tao Du[3]

**Abstract**

The emergence of distributed generators has changed the operational mode and fault characteristics of the distribution network, in a way which can severely influence protection. This paper proposes a d-axis-based current differential protection scheme. The d-axis current characteristics of inverter-interfaced distributed generators and synchronous generators are analyzed. The differential protection criterion using sampling values of the d-axis current component is then constructed. Compared to conventional phase-based current differential protection, the proposed protection reduces the number of required communication channels, and is suitable for distribution networks with inverter-interfaced distributed generators with complex fault characteristics. Finally, a 10 kV active distribution network model is built in the PSCAD platform and protection prototypes are developed in RTDS. Superior sensitivity and fast speed are verified by simulation and RTDS-based tests.

**Keywords:** Inverter-interfaced distributed generator, Active distribution network, D-axis current, Differential protection, Sampling value

## 1 Introduction

With increased numbers of distributed generators (DGs) being connected to the distribution network, the conventional network has become an active distribution network. The emergence of DGs has changed the power flow and fault current characteristics of the network. On the one hand, DGs cause bi-directional power flow and uncertain magnitude and direction of load current and fault current, while on the other, the output currents of DGs that use solar and wind energy fluctuate [1–3]. Because of the above factors, it is difficult to set the threshold value for conventional overcurrent protection, and its protection range, sensitivity and reliability are severely affected. Inverter-interfaced distributed generators (IIDGs) are widely used because of their flexible control strategy [4, 5]. However, IIDGs have more complicated fault characteristics than rotating-type distributed generators (RTDGs). Therefore, it is necessary to introduce a protection scheme for an active distribution network with different types of DGs. Recently, researchers have proposed three types of new protection schemes based on local, dual-terminal, and multi-terminal information.

Adaptive protection adjusts the threshold value in real-time under the current network topology to meet the protection requirements. In [6], an adaptive overcurrent protection scheme is proposed, where the fault currents for all the simulated faults are saved. If there is a significant change in the network, the optimum protection settings are established. However, because of fluctuations in DG output, frequent recalculation of the setting value is required and this can be time-consuming. If a fault occurs during this period, the correct operation of the protection may not be guaranteed. In [7], a directional distance relay is proposed. This needs to know the voltage and current to calculate the setting value of the impedance. However, the acquisition of voltage information is difficult in the existing distribution network.

Wide-area protection realizes the interaction of multi-terminal information through the smart terminal unit.

*Correspondence: guibinzou@sdu.edu.cn

[1] School of Electrical Engineering, Shandong University, Ji'nan, China
Full list of author information is available at the end of the article

In [8], a three-level hierarchically coordinated system is introduced to enable the protection. At the same time a backup protection strategy is proposed to solve the problem of communication interruption. In [9], the relay agents of different protected areas cooperate to perform protection function. However, wide-area protection has a high requirement on the reliability of communication, and highly depends on the stability of the master station. In addition, it cannot be extended to the entire distribution network.

To solve the problems in the above two types of protection, pilot protection schemes using peer-to-peer communication are proposed [10, 11]. Conventional phase-based current differential protection uses the three-phase current to construct a protection criterion but this increases the burden of communication, whereas the protection method in [12] based on negative-sequence current cannot reflect all types of faults. Consequently, some pilot protection schemes based on the ratio of the positive sequence currents at both ends of the protected section are proposed in [13, 14]. These rely on the amplitude difference between the two ends. However, the protection may fail in two cases, i.e., in the section with generators at two ends with large DG capacity on the load side, and when there is a fault with large transition resistance. For these problems, differential protection schemes based on current phasor are proposed in [15–17], while a protection scheme only using the phase angle is proposed in [18]. However, the phase angle of fault current supplied by an IIDG is related to the voltage at the point of common coupling (PCC). Thus, when an internal fault occurs in the section powered by the system-side generator and IIDG respectively, the angle difference of the positive-sequence currents at both ends can be 130° at most, which may lead to the failure of the protection scheme [19]. Impedance differential protection schemes are proposed in [20–23], but these schemes require voltage information, which as we have said is difficult to acquire in the existing distribution network. Based on the relationship between the current output characteristics of IIDG and the voltage drop, a virtual multi-terminal current differential protection scheme is proposed in [24], although it still faces the problem of voltage information acquisition.

Given the above problems, this paper analyzes the control strategy of an IIDG and its influences on the d-axis current characteristics of an IIDG. At the same time, the d-axis current characteristics of synchronous generators are also analyzed. A differential protection scheme based on the sampling value of d-axis current is constructed. A 10 kV active distribution network model is developed in PSCAD to verify the effectiveness of the proposed method. Finally, a protection prototype is developed and closed-loop tests using real-time digital simulator (RTDS) are carried out to further verify its practicability.

## 2 Fault characteristics of d-axis current

### 2.1 Control system of IIDG

As shown in Fig. 1, an IIDG converts DC into AC through a three-phase inverter. As shown, $u_{dc}$ is the DC voltage, $L$ is the AC side inductance, $C$ is the AC filter capacitor, while $L$ and $C$ form a $LC$ filter. $I_a$, $i_b$ and $i_c$ are the abc three-phase currents. $P_{ref}$ and $Q_{ref}$, $P_{AC}$ and $Q_{AC}$ are the reference values and actual output values of active power and reactive power on the AC side, respectively. $I_{dref}$, $i_{qref}$, $i'_{dref}$, $i'_{qref}$ are the reference values of the d-axis and q-axis currents before and after the current limiting module. $I_d$ and $i_q$, $e_d$ and $e_q$ are the actual output values of the d-axis and q-axis components of current and voltage on the AC side, respectively.

An IIDG generally adopts a constant power (PQ) control mode. This is realized by a double closed-loop control strategy, including the outer power loop and the inner current loop [25]. The outer loop aims to control the power and generates the reference currents for the inner current loop control. The inner loop controller generates the SPWM modulation signal to track the current commands. To realize the decoupling control of P and Q and simplify the design of the control system, AC in the static abc coordinate system is usually converted to DC in the synchronous rotating dq coordinate system [26]. Thus, in an IIDG, the d-axis current controls the active power P and the q-axis current controls the reactive power Q.

In addition, an IIDG also has other control strategies, which make the fault characteristics of an IIDG different from the RTDG, e.g.:

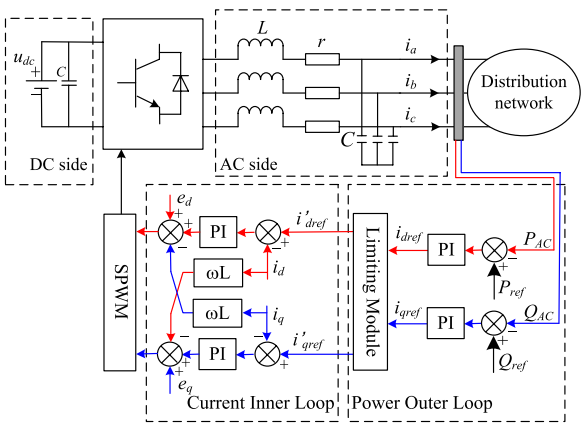


**Fig. 1** Schematic diagram of IIDG control system

- The overcurrent control requires that the maximum output current of the IIDG is only 1.2-2 times the rated current;
- The elimination of the negative sequence current control requires the output current of the IIDG to only contain a positive-sequence component even if an asymmetrical fault occurs in the feeder;
- Low voltage ride through (LVRT) control requires the IIDG to continue grid-connected operation after detecting the voltage drop at PCC for voltage support.

### 2.2 D-axis current characteristics of an IIDG

After a fault occurs at a feeder, the voltage at the PCC can drop sharply. Different voltage drops at the PCC lead to different control strategies of the IIDG. Generally, the IIDG mainly undergoes two processes after the occurrence of the fault: constant power control and LVRT control.

#### *2.2.1 Current change of IIDG under constant power control*

When the voltage at the PCC after the fault ($|\dot{U}_f|$) is larger than 0.9 times of the pre-fault value ($0.9|\dot{U}_{nor}|$), the IIDG is still in constant power control. At this time, to achieve maximum power point tracking, the power factor of the IIDG is 1, and the d-axis component of the fault current ($\dot{I}_{d.f}$) and the q-axis component of the fault current ($\dot{I}_{q.f}$) are given as:

$$\begin{cases} |\dot{I}_{d.f}| = P_{ref}/|\dot{U}_f| \\ \dot{I}_{q.f} = 0 \end{cases} \tag{1}$$

It can be seen from (1) that when the IIDG is in constant power control, the d-axis current increases with the decrease of the voltage at PCC, and the q-axis current is always 0.

#### *2.2.2 Current change of IIDG under LVRT control*

When the IIDG detects that $|\dot{U}_f|$ has dropped below $0.9|\dot{U}_{nor}|$, LVRT control starts. According to the requirements of LVRT, the IIDG gives priority to output reactive current (q-axis current) during the fault to support the AC voltage. Meanwhile, to ensure the balance of active power of the grid, the IIDG needs to output as much active current (d-axis current) as possible within the capability of the inverter. The fault current output characteristics of the IIDG are given as:

$$\begin{cases} \dot{I}_f = \dot{I}_{d.f} + \dot{I}_{q.f} \\ |\dot{I}_{d.f}| = min\left\{ P_{ref}/\left|\dot{U}_f\right|, \sqrt{I_{max}^2 - \left|\dot{I}_{q.f}\right|^2} \right\} \\ |\dot{I}_{q.f}| = min\left\{ k_q\left|\dot{U}_{nor} - \dot{U}_f\right|, I_{max} \right\} \end{cases} \tag{2}$$

where $\dot{I}_f$ is the fault current, $k_q$ is the reactive power support coefficient, and $I_{max}$ is the maximum current allowed by the IIDG. From (2), the output current of the IIDG is related to the drop of the voltage after a feeder fault. The current phasor after the feeder fault is further illustrated in Fig. 2.

Based on the analysis in Sect. 2.2.1, when $|\dot{U}_f|>0.9|\dot{U}_{nor}|$, the output power factor of IIDG is 1 to make full use of energy generation, i.e., the output current of IIDG ($\dot{I}_{nor}$) only contains the d-axis component ($\dot{I}_{d.nor}$), and $\dot{I}_{d.nor} = \dot{I}_{nor}$ After the fault, $\dot{U}_f$ has a $\beta$ angle offset relative to $\dot{U}_{nor}$. The output characteristic of $\dot{I}_f$ is related to the IIDG control strategy, and it rotates in a fan-shaped area whose radius is $I_{max}$, as shown by the dotted line in Fig. 2a. $\dot{I}'_f$ and $\dot{I}''_f$ correspond to the different output states of $\dot{I}_f$. In the following, $\dot{I}'_{d.f}$, $\dot{I}''_{d.f}$ represent the d-axis currents for different voltage drops. Controlled by LVRT, the angle between $\dot{I}_f$ and $\dot{U}_f$ increases with $|\dot{U}_f|$ decreasing. In the fan-shaped area in red shown in Fig. 2a, $|\dot{I}_{d.f}|>|\dot{I}_{d.nor}|$, while in the fan-shaped area in blue in Fig. 2b, $|\dot{I}_{d.f}|<|\dot{I}_{d.nor}|$. When the angle between $\dot{I}_f$ and $\dot{U}_f$ rotates from 0° to 90°, there is a critical state that $|\dot{I}_{d.f}|=|\dot{I}_{d.nor}|$, and the q-axis current $\dot{I}_{q.f}$ satisfies:

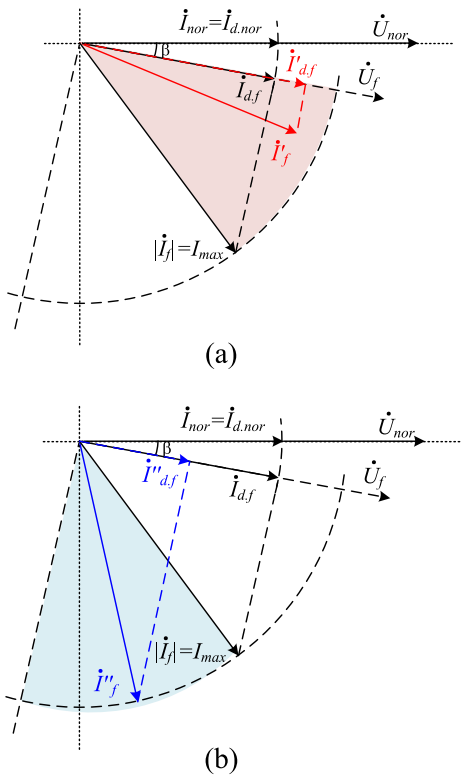


**Fig. 2** Output current phasor of IIDG: **a** When the voltage drop is small; **b** When the voltage drop is large

$$|\dot{I}_{q.f}| = I_{max} sin\left(arccos\frac{|\dot{I}_{nor}|}{I_{max}}\right) \tag{3}$$

From the requirements of the grid connection regulations, when the voltage drop exceeds 10%, for every 1% voltage drop, at least 2% of the q-axis current needs to be provided to support the voltage, i.e., the current output of IIDG is controlled as:

$$\frac{0.9|\dot{U}_{nor}| - |\dot{U}_f|}{|\dot{U}_{nor}|} : \frac{|\dot{I}_{q.f}|}{I_{max}} = 1:2 \tag{4}$$

The relationship between the critical voltage value $U_{f.0}$ and $\dot{U}_{nor}$ is further derived from (3)–(4), as:

$$U_{f.0} = \left[0.9 - 0.5 sin(arccos(|\dot{I}_{nor}|/I_{max}))\right] \cdot |\dot{U}_{nor}| \tag{5}$$

Affected by the current limiting module in the IIDG control system, $I_{max} \in (1.2|\dot{I}_{nor}|, 2|\dot{I}_{nor}|)$. In this paper: $I_{max}=1.2|\dot{I}_{nor}|$, and (5) can be simplified as $U_{f.0}=0.624|\dot{U}_{nor}|$. Thus, when the voltage drop is small, $|\dot{U}_f|>0.624|\dot{U}_{nor}|$, and $|\dot{I}'_{d.f}|$ increases compared with $|\dot{I}_{d.nor}|$. In addition, when $|\dot{U}_f|>0.624|\dot{U}_{nor}|$, the situation of $|\dot{I}'_f|=I_{max}$ exists, $\dot{I}'_{q.f}$ satisfies (4) while $\dot{I}'_{d.f}$ satisfies:

$$|\dot{I}'_{d.f}| = P_{ref}/|\dot{U}_f| \tag{6}$$

From (4) and (6), it can be deduced that $|\dot{I}'_f|=I_{max}$ when $|\dot{U}_f|=0.84|\dot{U}_{nor}|$.

When $|\dot{U}_f|<0.624|\dot{U}_{nor}|$, $\dot{I}''_f$ rotates in the fan-shaped area in blue in Fig. 2b, and $|\dot{I}_{d.f}|<|\dot{I}_{d.nor}|$, $|\dot{I}''_f|=I_{max}$. In such a condition, $I'_{q.f}$ satisfies (4), while $I'_{d.f}$ satisfies:

$$\left|\dot{I}''_{d.f}\right| = \sqrt{I^2_{\max} - \left|\dot{I}''_{d.f}\right|^2} \tag{7}$$

From (4) and (7), it can be seen that when $|\dot{U}_f|=0.4|\dot{U}_{nor}|$, the critical state of $|\dot{I}_{q.f}|=I_{max}$ is reached. When the voltage drop exceeds 60%, $|\dot{U}_f|<0.4|\dot{U}_{nor}|$, $|\dot{I}''_{d.f}|=0$.

The changes of the d-axis current with different voltage drops at the PCC are shown in Fig. 3.

The angle γ of the output current supplied by IIDG is:

$$\gamma = \arctan(|\dot{I}_{q.f}|/|\dot{I}_{d.f}|) \tag{8}$$

From the analysis above, γ varies from 0° to 90° under different voltages at the PCC. As the condition of faults is unpredictable, consequently, γ is random.

### 2.3 D-axis current characteristics of synchronous motors

Synchronous generators, which have similar fault characteristics to RTDGs, are the main power source of the distribution network. To correspond with the output characteristics of an IIDG and simplify the analysis of the fault characteristics of an active distribution network,

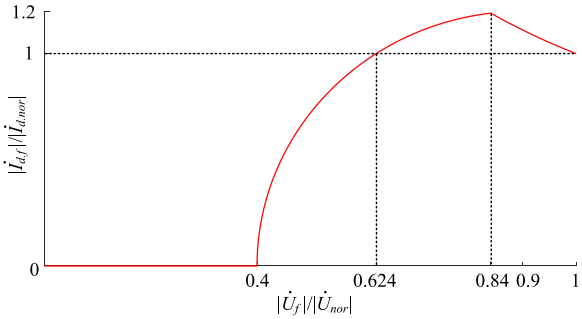


**Fig. 3** Changes of d-axis current with different voltage drops at the PCC

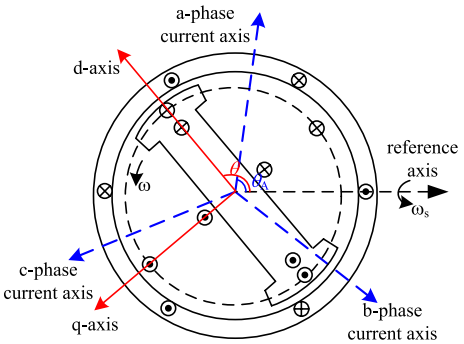


**Fig. 4** Relative position of the dq-axis and the abc three-phase current axis in the synchronous generator

the Park Transform is used to convert the abc-aixs current into the dq0-axis current. The relative positions of the dq-axis and the abc-axis in the synchronous generator are shown in Fig. 4. In Fig. 4, $\omega_s$ is the angular velocity of the rotating magnetic field of the stator winding, ω is the angular velocity of the rotor, and $\omega_s = \omega$ in a synchronous generator. $I_{am}$, $I_{bm}$, $I_{cm}$ represent the respective amplitudes of the three-phase current, and $\theta_A$ is the initial angle between the a-phase current axis and the reference axis. Thus, the three-phase current can be expressed as sine functions varying with time, as:

$$\begin{cases} I_a = I_{am} sin(\omega t + \theta_A) \\ I_b = I_{bm} sin(\omega t + \theta_A - 2\pi/3) \\ I_c = I_{cm} sin(\omega t + \theta_A + 2\pi/3) \end{cases} \tag{9}$$

According to the Park Transformation, the dq-axis current can be obtained from the abc-axis current, as:

$$\begin{bmatrix} I_d(k) \\ I_q(k) \end{bmatrix} = P_{Iabc} \cdot \begin{bmatrix} I_a(k) \\ I_b(k) \\ I_c(k) \end{bmatrix} \tag{10}$$

$$P_{Iabc} = \frac{2}{3}\begin{bmatrix} \cos(\phi) & \cos(\phi - \frac{2}{3}\pi) & \cos(\phi + \frac{2}{3}\pi) \\ -\sin(\phi) & -\sin(\phi - \frac{2}{3}\pi) & -\sin(\phi + \frac{2}{3}\pi) \end{bmatrix} \tag{11}$$

$$\phi = k\omega \triangle t + \theta \tag{12}$$

In (10)–(12), $I(k)$ is the current value of the $k$-th sampling point, $P_{Iabc}$ is the Park Transformation matrix, $\Delta t$ is the sampling interval, and $\theta$ is the angle between the d-axis and the reference axis in the initial state. The key element of the Park Transformation is the introduction of a time-varying rotation angle $k\ \omega\ \Delta t$ to construct a rotating coordinate system. This shows that the sampling values at different moments correspond to different transformation angles.

From (9)–(12), the relationship between the d-axis current $I_d$ and the three-phase current can be further derived as:

$$\begin{aligned} I_d =& 1/3\{[I_{am} + I_{bm} + I_{cm}]\ \sin(\theta_A - \theta) \\ &+ \left[I_{am} - (I_{bm} + I_{cm})/2\right] \sin(2\omega t + \theta_A + \theta) \\ &+ \left[\sqrt{3}(I_{bm} - I_{cm})/2\right] \cos(2\omega t + \theta_A + \theta)\} \end{aligned} \tag{13}$$

Under normal conditions, the system is in a three-phase symmetrical state, and the amplitudes of the three-phase currents are equal, i.e., $I_{am}$=$I_{bm}$=$I_{cm}$. In this case, $I_d$ =[($I_{am}$+$I_{bm}$+$I_{cm}$) *sin* ($\theta_A$ —$\theta$)]/3. As $I_{am}$, $I_{bm}$, $I_{cm}$, θ, $\theta_A$ are all constant values, $I_d$ becomes a DC quantity [27].

When a symmetrical fault occurs in the feeder, the three-phase system remains symmetrical once reaching steady state during the fault, $I_{am}$, $I_{bm}$, $I_{cm}$ increase symmetrically, and thus $I_d$ increases. Under such a condition, $I_d$ is equivalent to changing from one DC state to another DC state with a larger amplitude.

When an asymmetrical fault occurs in the feeder, $I_{am}$, $I_{bm}$, $I_{cm}$ are not equal after reaching steady state during the fault. The phase current increases, $I_d$ increases but contains a double frequency component. Thus, $I_d$ is equivalent to changing from the DC state to the double frequency AC state.

Figure 5 shows the characteristics of $I_d$ when different types of faults occur. As can be seen, when the fault occurs at 0.4 s, regardless of the fault type, $I_d$ increases rapidly and enters into another DC state or double frequency AC state. Assuming that the phase-a current axis coincides with the d-axis in the initial state, $\theta$=$\theta_A$, $I_d$ =0. Thus, $I_d$ can be considered to only appear after a fault, which means $I_d$ has similar properties to the fault component and contains an obvious fault characteristic.

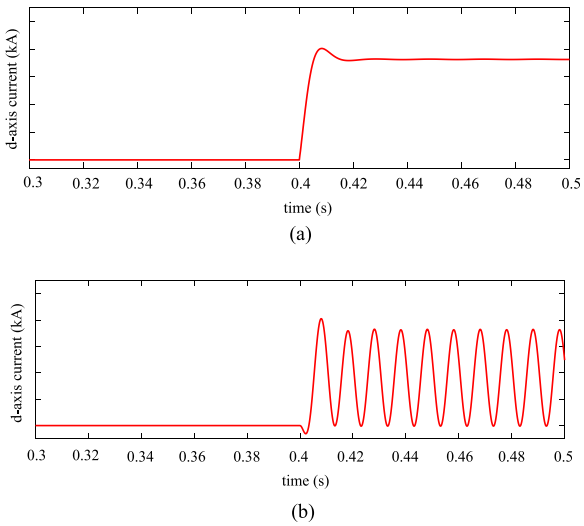


**Fig. 5** D-axis current waveforms of synchronous motor after the fault (**a**) Symmetrical fault (**b**) Asymmetrical fault

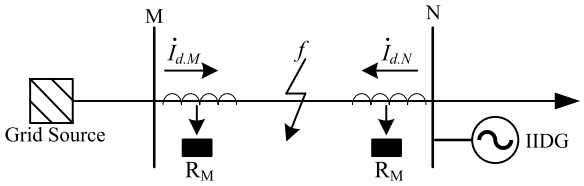


**Fig. 6** Simple active distribution network

## 3 D-axis current-based differential protection

Figure 6 shows a simple active distribution network, where $R_M$ and $R_N$ are relays that perform the protection function. They are installed on the system side and the load side, respectively. $\dot{I}_{d.M}$ and $\dot{I}_{d.N}$ represent the respective positive directions of the d-axis currents flowing through $R_M$ and $R_N$.

Based on Kirchhoff's current law, and referring to the form of conventional ratio differential protection, a novel differential protection criterion based on the d-axis current is constructed.

Under normal conditions, based on Kirchhoff's current law, $|\dot{I}_{d.M}+\dot{I}_{d.N}|=0$, $|\dot{I}_{d.M}+\dot{I}_{d.N}|<|\dot{I}_{d.M}-\dot{I}_{d.N}|$. When an internal metallic short-circuit fault occurs, $\dot{I}_{d.M}$ and $\dot{I}_{d.N}$ are provided by the synchronous generator on the system side and IIDG on the load side with the same direction, respectively. Under this condition, $|\dot{I}_{d.M}+\dot{I}_{d.N}|>|\dot{I}_{d.M}-\dot{I}_{d.N}|$.

According to the analysis in Sect. 2, $|\dot{I}_{d.N}|$ increases in a short time after the fault under constant power control. The increase of $|\dot{I}_{d.N}|$ is conducive to the establishment of the relationship $|\dot{I}_{d.M}+\dot{I}_{d.N}|>|\dot{I}_{d.M}-\dot{I}_{d.N}|$. In this process, if IIDG detects $|\dot{U}_f|<0.9|\dot{U}_{nor}|$,

it will perform LVRT control. When $0.624|\dot{U}_{nor}|<|\dot{U}_f|<0.9|\dot{U}_{nor}|$, the gap between $|\dot{I}_{d.M}+\dot{I}_{d.N}|$ and $|\dot{I}_{d.M}-\dot{I}_{d.N}|$ increases whereas $\dot{I}_{d.N}$ decreases as $|\dot{U}_f|$ decreases for $0.4|\dot{U}_{nor}|<|\dot{U}_f|<0.624|\dot{U}_{nor}|$. The d-axis current supplied by IIDG is reduced to 0, when $|\dot{U}_f|<0.4|\dot{U}_{nor}|$, and the active distribution network can be regarded as a network powered only by the grid-side source. In this condition, $\dot{I}_{d.N}$ is the crossing current provided by the grid source, and is affected by the upstream equivalent impedance, transition resistance, downstream line impedance, and load impedance. The relationship between $\dot{I}_{d.M}$ *and* $\dot{I}_{d.N}$ can be expressed as: $\dot{I}_{d.N}=\alpha\ \dot{I}_{d.M}$, $|\dot{I}_{d.M}+\dot{I}_{d.N}|\approx|\dot{I}_{d.M}|-|\alpha\ \dot{I}_{d.M}|$, $|\dot{I}_{d.M}-\dot{I}_{d.N}|\approx|\dot{I}_{d.M}|+|\alpha\ \dot{I}_{d.M}|$, where α is the branch coefficient and is related to the network topology parameters after the fault. In this case, the restraint coefficient $K_{res}$ ($K_{res}<1$) is introduced to ensure that the relationship of $|\dot{I}_{d.M}+\dot{I}_{d.N}|>|\dot{I}_{d.M}-\dot{I}_{d.N}|$ is still valid.

The selection of $K_{res}$ will affect the sensitivity of the proposed protection scheme. To improve the sensitivity for an internal fault, the value of $K_{res}$ needs to be low. On the contrary, to improve the reliability of the protection for an external fault, the value of $K_{res}$ needs to be high. In fact, the selection of $K_{res}$ may use the margin of external faults to ensure the reliability in the case of internal faults. Therefore, it is necessary to comprehensively consider the influence of branch load and transition resistance. According to Kirchhoff's law, the value of $|\dot{I}_{d.M}+\dot{I}_{d.N}|$ is almost 0 when an external fault occurs, and there is a large difference between $|\dot{I}_{d.M}-\dot{I}_{d.N}|$ and $|\dot{I}_{d.M}+\dot{I}_{d.N}|$. Thus, the margin can be used to choose a suitable value of $K_{res}$. The purpose of the arrangement is to ensure the effectiveness when the voltage at the PCC drops severely and when a fault with a large transition resistance occurs. In this paper, $K_{res}=0.2$.

In addition, to obtain the d-axis current, it is necessary to perform a coordinate transformation of different angles for each sampled value. To affect this, the differential current ($I_{diff}$) and the restraint current ($I_{res}$) based on the d-axis current sampling value are defined as:

$$I_{diff}(k) = \left|I_{d.M}(k) + I_{d.N}(k)\right| \tag{14}$$

$$I_{res}(k) = K_{res} \cdot \left|I_{d.M}(k) - I_{d.N}(k)\right| \tag{15}$$

Ignoring the influence of the crossing current, $\dot{I}_{d.N}$ is completely provided by IIDG. From the protection criterion shown in (14)–(15), when an internal fault occurs, the large value of $\dot{I}_{d.N}$ is beneficial to the judgment of the faulty section. This means, if RTDG is connected to the distribution network, the performance of the proposed criterion is better than with IIDG. Therefore, to verify its effectiveness, the simulation and prototype test carried out in Sects. 4 and 5 will be based on the distribution network model with IIDG.

We assume that the protection criterion based on a single sampling point is easily affected by the fault initiation angle and noise, and the sums of $I_{diff}$ and $I_{res}$ of all sampling points in a time window are calculated to identify the faulty section. Each data window includes X sampling points, and the cumulative differential current ($S_{diff}$) and restraint current ($S_{res}$) can be expressed as:

$$S_{diff} = \sum_{k=x}^{x+X-1} I_{diff}(k) \tag{16}$$

$$S_{res} = \sum_{k=x}^{x+X-1} I_{res}(k) \tag{17}$$

When $S_{diff}>S_{res}$, an internal fault is identified. To ensure the speed and reliability of the protection scheme, half a cycle is selected as the length of the time window. According to the analysis in Sect. 2, when an asymmetric fault occurs, the d-axis current is double-frequency AC. Therefore, in a 50 Hz system, 5 ms is selected as the length of the time window. The flow chart of the protection scheme is shown in Fig. 7.

The proposed protection scheme is based on Kirchhoff's current law, and its theoretical basis is that the currents at both ends of the section are synchronized in the same reference coordinate system. In practice, the periodically changing phase angle obtained by the bus voltage through PLL is often used as the rotation angle of the Park Transformation. However, considering the lack of voltage transformers in distribution networks and the oscillation of voltage after fault occurrence, voltage is only used to calculate the initial phase angle $\theta_0$, and then $k\omega\Delta t+\theta_0$ is selected as the rotation angle $\phi$ in the

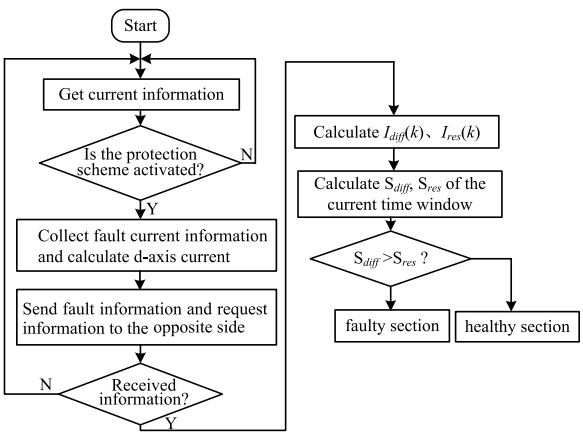


**Fig. 7** Flow chart of the protection scheme

proposed scheme. To ensure that the calculation results of the d-axis current are in the same coordinate system, the rotation angle of the sampling point at the same time should be equal. Due to the complex topology of the distribution network and a large number of branches, the cost of installing GPS at every node is high. Therefore, a built-in time synchronization algorithm in the relay is a more economical solution to this problem.

Compared with the phasor-based protection schemes, this sample-based protection scheme does not require a Fourier Transform, so has an excellent performance in terms of speed. In addition, the proposed protection is suitable for distribution networks with an IIDG in which γ is random, while it also reduces the burden of communication compared with conventional three-phase current differential protection. Also, it has no requirement for voltage transducers, which reduces investment cost.

## 4 Simulation analysis

### 4.1 Simulation model

To verify the effectiveness of the proposed protection scheme, the simplified active distribution network model shown in Fig. 8 is used. Sections $N_1N_3$ and $N_3N_4$ are powered by double-sided sources, and therefore conventional overcurrent protection schemes may not be applicable. In the proposed protection method, relays are arranged at both ends of the sections to identify the faulty section, while $R_3$–$R_6$ are relays that perform the protection function. In China, the 10 kV distribution network is neutral ungrounded. Thus, when single-phase grounding faults occur, the system can continue to operate for 2 hours. Therefore, only the phase-to-phase faults are simulated.

The system reference voltage is 10.5 kV, the reference capacity is 200 MVA, and the IIDG capacity is 1 MW. $f_1$–$f_5$ are located at the midpoints of sections $N_1N_2$, $N_1N_3$, $N_3N_4$, $N_4N_5$, and $N_1N_6$, respectively. The feeders are mixed configurations of cables and overhead lines. The lengths of feeders 1–3 are 3.75 km, 12.93 km, and 2.78 km, respectively. Section $N_1N_2$ is entirely composed of overhead lines with length of 1.87 km. Sections $N_1N_3$, $N_3N_4$ $N_4N_5$, and $N_1N_6$ are entirely composed of cables, with lengths of 0.7 km, 0.8 km, 5.42 km, and 2.78 km, respectively. In the simulation, section $N_3N_4$ is taken as the object to be studied, and feeder 2 is drawn in detail in Fig. 8 while the other feeders are simplified as lines and loads. In the simulation, $K_{res} = 0.2$, the sampling frequency is 5 kHz, the system frequency is 50 Hz, and the time window length is 5 ms.

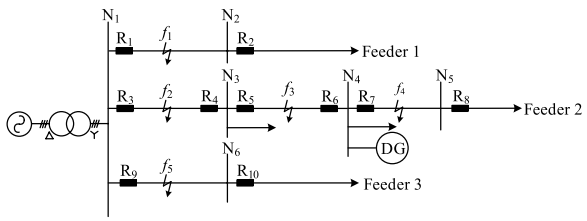


**Fig. 8** Active distribution network model with IIDG

### 4.2 External faults

Three-phase short-circuit external faults are set at $f_1$, $f_2$, $f_4$ and $f_5$ respectively to verify the effectiveness of the proposed protection scheme. The faults occur at 0.4s, and $S_{diff}$ and $S_{res}$ are calculated according to (14)–(17). The simulation results are shown in Table 1 and Fig. 9.

As shown, for external three-phase faults, $S_{res}$ increases while $S_{diff}$ only has small changes, and $S_{diff}$ is much smaller than $S_{res}$. The results verify that the proposed protection scheme will not make a misjudgment when severe three-phase short-circuit external faults occur.

### 4.3 Internal faults

Symmetric short-circuit faults are set at $f_3$, and the results are shown in Fig. 10. It can be seen that, for an internal three-phase fault, both $S_{diff}$ and $S_{res}$ increase, but $S_{diff}$ is much larger than $S_{res}$, which meets the protection criteria within a very short time. The protection scheme can reliably distinguish the faulty section from the healthy sections.

Asymmetric faults are also applied at $f_3$, including a two-phase fault and a two-phase-to-ground fault (without or with transition resistance $R_f$). The simulation results are listed in Table 2.

As can be seen from Table 2, the proposed protection scheme can correctly identify the faulty section for internal faults. When a two-phase-to-ground internal fault

**Table 1** Simulation results of $N_3N_4$ for three-phase short-circuit external faults

| Fault location | $S_{diff}$/kA | $S_{res}$/kA | Result |
|---|---|---|---|
| $f_1$ | 0.010 | 0.057 | External fault |
| $f_2$ | 0.032 | 0.776 | External fault |
| $f_4$ | 0.013 | 24.99 | External fault |
| $f_5$ | 0.008 | 0.046 | External fault |

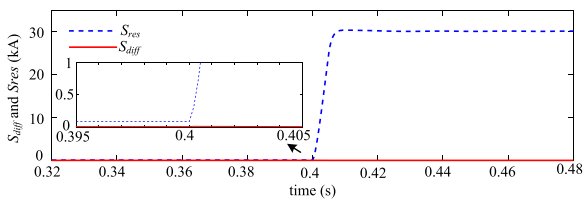


**Fig. 9** Protection performance for fault at $f_4$

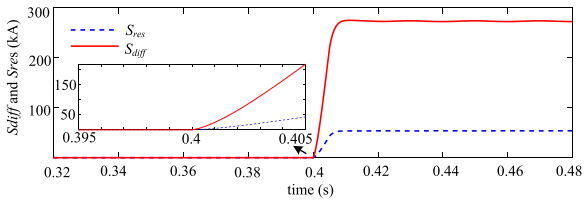


**Fig. 10** Protection performance for fault occurring at $f_3$

**Table 2** Simulation results of $N_3N_4$ when asymmetric faults occur at $f_3$

| Fault type | $R_f$ /(Ω) | $S_{diff}$ /kA | $S_{res}$ /kA | Result |
|---|---|---|---|---|
| Two-phase | 0 | 134.07 | 26.41 | Internal fault |
| Two-phase-ground | 0 | 127.57 | 25.17 | Internal fault |
| | 5 | 18.77 | 3.78 | Internal fault |
| | 50 | 2.22 | 0.52 | Internal fault |

**Table 3** Simulation results of internal faults occurring at the beginning and the end of $N_3N_4$

| Fault location | Fault type | $S_{diff}$ /kA | $S_{res}$ /kA | Result |
|---|---|---|---|---|
| $f_3'$ | ABC | 256.79 | 50.71 | Internal fault |
| | AB | 158.13 | 31.21 | Internal fault |
| | AB-g | 148.81 | 29.42 | Internal fault |
| $f_3''$ | ABC | 194.70 | 38.29 | Internal fault |
| | AB | 116.47 | 22.87 | Internal fault |
| | AB-g | 111.75 | 21.97 | Internal fault |

with a large transition resistance (e.g., 50 Ω) occurs, the sensitivity is slightly reduced, but the proposed scheme is still reliable with a sensitivity coefficient greater than 1.5. Therefore, the proposed protection scheme is suitable for short-circuit ground fault situations with large transition resistance.

As the distance between the fault point and the PCC will affect the voltage at the PCC, which indeed affects the current fault characteristics of the IIDG, three types of faults are set at different distances from the PCC and the results are shown in Table 3. $f_3'$ and $f_3''$ are located at 1% and 99% from section $N_3N_4$, respectively. According to Table 3, the change of the fault location has little effect on the sensitivity of the protection scheme. Even if the fault occurs at the beginning or the end of the protected section, the protection scheme can still identify the faulty section correctly.

In summary, the protection scheme can correctly reflect all the fault types at different locations of the feeder fast and with superior sensitivity. Also, the scheme is less affected by the transition resistance.

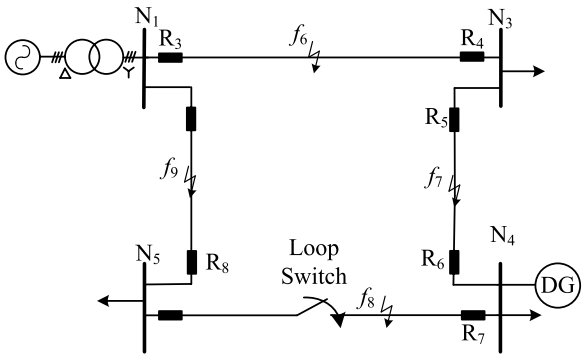


**Fig. 11** Active distribution network model in closed loop

**Table 4** Simulation results of $N_3N_4$ in closed loop network model when external faults occur

| Fault location | $S_{diff}$ /kA | $S_{res}$/kA | Result |
|---|---|---|---|
| $f_6$ | 0.011 | 9.692 | External fault |
| $f_8$ | 0.012 | 23.287 | External fault |
| $f_9$ | 0.014 | 6.588 | External fault |

**Table 5** Simulation results of $N_3N_4$ in closed loop network model when internal faults occur at $f_7$

| Fault type | $R_f$ /(Ω) | $S_{diff}$ /kA | $S_{res}$ /kA | Result |
|---|---|---|---|---|
| Three-phase | 0 | 246.146 | 34.430 | Internal fault |
| Two-phase | 0 | 152.949 | 21.421 | Internal fault |
| Two-phase-ground | 0 | 143.238 | 20.011 | Internal fault |
| | 5 | 18.437 | 2.423 | Internal fault |
| | 50 | 2.115 | 0.175 | Internal fault |

### 4.4 Simulation results under closed-loop model

A further simulation is conducted of the looped distribution network as shown in Fig. 11 [28]. The parameters in Fig. 11 are the same as those of feeder 2 in Fig. 8.

Section $N_3N_4$ is selected for study and three-phase short-circuit faults are set at $f_6$, $f_8$ and $f_9$ to verify the effectiveness in the case of severe external faults, while different types of internal faults with different transition resistances are set at $f_7$. Simulation results are shown in Tables 4 and 5. Similar to the simulation results of the open-loop network, the results show that the proposed protection scheme can correctly distinguish the faulty section in the closed loop network model.

### 4.5 Simulation results for single-phase grounding faults

To verify the performance of the proposed protection method under a single-phase grounding fault, the neutral point of the distribution network model in Fig. 8 is

**Table 6** Simulation results of $N_3N_4$ when single-phase grounding faults occur at $f_3$

| Fault phase | $R_f$ /(Ω) | $S_{diff}$ /kA | $S_{res}$ /kA | Result |
|---|---|---|---|---|
| A | 0 | 17.793 | 3.494 | Internal fault |
| B | 50 | 1.830 | 0.456 | Internal fault |
| C | 100 | 0.461 | 0.167 | Internal fault |

grounded. Section $N_3N_4$ is also selected for study, and internal single-phase grounding faults are applied. The simulation results in Table 6 show that the proposed protection method is reliable for single-phase grounding faults in the distribution network with neutral grounding.

## 5 Prototype development and testing

To further verify the speed and practicability of the proposed protection scheme, based on the protection criterion described above, relay prototypes with protection functions are developed. They can monitor the three-phase current of the feeder in real-time and have a time synchronization function. They adopt a sudden change of phase current to start, and when the currents of three consecutive sampling points meet (18), the relay prototypes activate. In (18), $i(t)$ is the sampling value of phase current at time $t$, T is the power frequency period, and $I_N$ is the rated current.

$$\|i(t)-i(t-T)|-|i(t-T)-i(t-2T)\| \geq 0.1I_N \tag{18}$$

In addition, the relay prototypes adopt a ping-pong time synchronization algorithm, and start to perform the time synchronization before entering the differential protection calculation. When the time error is less than a sampling interval, the fault identification program is executed.

### 5.1 Prototype development and platform construction

The prototype is composed of four plug-in boards: power supply/open-in board, acquisition board, open-out board, and management board. The management board is the core of the prototype and has functions such as data processing and logic control, mainly composed of two parts: the programmable logic device FPGA and the AM5716 processor. The FPGA collects data of each analog quantity channel, while the AM5716 performs data processing and storage functions, and realizes data interaction with the FPGA.

The RTDS closed-loop test platform is shown in Fig. 12. The information in the simulation model is output through the GTAO board of the RTDS, and is connected to the acquisition board of the prototype through the power amplifier. After the collected analog signals have undergone low-pass filtering and analog-to-digital conversion, the management board performs data processing. Then, the signals are sent out through the open-out board, which is connected to the GTFPI board of the RTDS to control the switch on and off of the simulation model. At the same time, the GTFPI board outputs the switch control signal to the relay, which is connected to the power supply/open in the board of the prototype to feedback the switch status. Adjacent prototypes rely on optical fiber communication.

### 5.2 RTDS closed loop test

The active distribution network model in Fig. 8 is built in RTDS, and relay prototypes are arranged at both ends of section $N_3N_4$. Internal faults are set at $f_3$ and various types of faults are tested for 15 times. The operation time of the prototype is shown in Fig. 13 and Table 7.

It can be seen from Fig. 13 and Table 7 that when a two-phase-to-ground fault with a large transition resistance occurs, the operation time of the prototype will increase slightly, but all can operate quickly within 20 ms. In comparison, the protection schemes proposed in [15, 16, 29] operate in the case of internal faults within 50 ms, 47 ms and 60 ms, respectively. This indicates that the protection scheme proposed is faster than the others.

The currents on both ends of the section $N_3N_4$ and the operation of relays under different conditions are shown in Figs. 14 and 15, where the three-phase currents flowing through $R_5$ and $R_6$ and the operation of $R_5$ and $R_6$ are recorded. For $R_5$ and $R_6$, "1" means that the switch is closed, and "0" is the operation signal to open the switch.

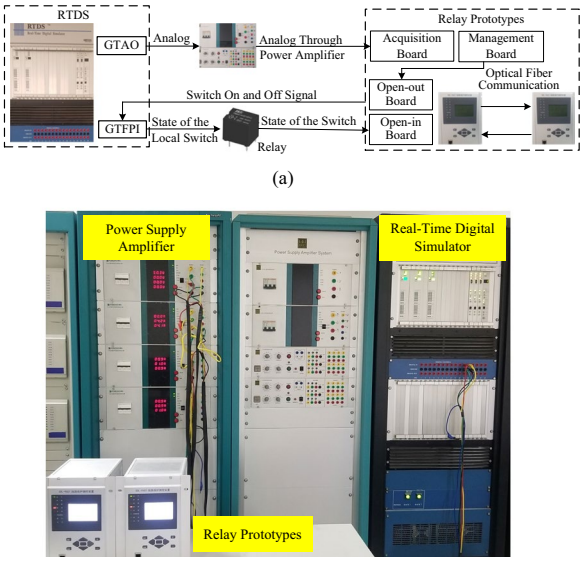


**Fig. 12** Test platform structure: **a** Schematic; **b** Actual photos

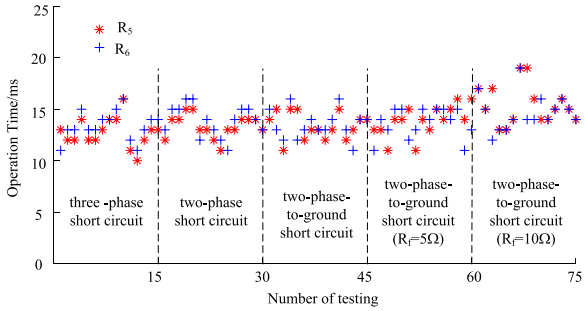


**Fig. 13** Operation time of the prototype

**Table 7** Average operation time under different fault conditions

| Fault type | Operation time/ms | |
|---|---|---|
| | $R_5$ | $R_6$ |
| Three-phase short-circuit | 12.73 | 13.40 |
| Two-phase short-circuit | 13.33 | 13.87 |
| Two-phase-to-ground short-circuit | 13.40 | 13.53 |
| Two-phase-to-ground short-circuit ($R_f$=5Ω) | 15.40 | 13.67 |
| Two-phase-to-ground short-circuit ($R_f$=10Ω) | 15.40 | 14.73 |

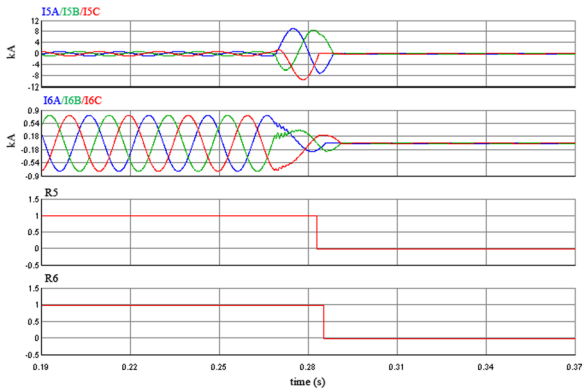


**Fig. 14** Fault record for an internal three-phase fault of section $N_3N_4$

The results show that the developed relay prototypes can quickly distinguish the faulty section from the healthy sections.

## 6 Conclusion

This paper analyzes the d-axis current characteristics of a synchronous generator and IIDG under fault conditions, and proposes a novel differential protection scheme based on the d-axis current. The scheme uses the sampling values of the d-axis currents at both ends of the section to calculate the differential and restraint currents, and accumulates sampling point information

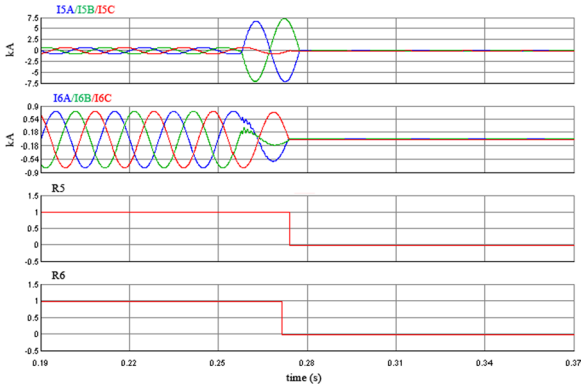


**Fig. 15** Fault record for an internal phase A to B fault of section $N_3N_4$

to improve reliability. Through theoretical analysis, simulation verification, and RTDS closed-loop testing, the following conclusions can be drawn:

(1) The fault characteristics of an IIDG are complex, and conventional protection schemes face challenges. In response to this problem, a novel current differential protection scheme based on d-axis current is proposed.
(2) The simulation results show that the proposed protection scheme can correctly identify the faulty section and reflect all fault types, and is applicable under large transition resistance. However, when an internal three-phase short-circuit fault occurs, the voltage at the PCC drops significantly and the d-axis current supplied by the IIDG may become 0. In this case, the effectiveness of the protection method depends on the restraining coefficient.
(3) The results from RTDS closed-loop tests show that the protection prototype is able to operate quickly within 20 ms in the event of an internal fault.
(4) Compared with conventional phase-current-based differential protection schemes, the proposed scheme only needs to transmit the d-axis current. This reduces the burden of communication.

**Abbreviations**

DG: Distributed generator; IIDG: Inverter-interfaced distributed generator; RTDG: Rotating-type distributed generator; PCC: Point of common coupling; RTDS: Real-time digital simulator; LVRT: Low voltage ride through.

**Acknowledgements**

The authors are grateful to Maoran Zheng (Power Dispatching and Control Center, China Southern Power Grid) for providing the model and parameters. The authors are also grateful to Tao Du (Shandong Shanda Electric Power Technology Co. LTD), for his help in the development of protection prototypes.

**Authors' information**
**G. B. Zou** (1971-), male, Ph.D. and Professor, Major in protection and control techniques of AC/DC grids, the protection of active distribution networks, and distribution system automation.
**C. H. Zhou** (1994-), male, Ph.D. candidate, Major in power system control and protection and active distribution networks.
**M. R. Zheng** (1981-), male, Major in power system control and protection.
**T. Du** (1975-), male, Major in power system control and protection.

**Author contributions**
LZ, the main author of this study, her contributions included the idea, mathematical and practical design, case study and writing the paper. GZ, the corresponding author, he guided the study at all stage and improved the text. CZ, MZ and TD are the supervisors of the study, they reviewed and improved the text. The author(s) read and approved the manuscript.

**Funding**
This work was supported by China Southern Power Grid Technology Project.

**Availability of data and materials**
All data used or analyzed during this study are included in the published article.

## Declarations

**Competing interests**
The authors declare that they have no known competing financial interests or personal relationships that could have appeared to influence the work reported in this paper.

**Author details**
[1]School of Electrical Engineering, Shandong University, Ji'nan, China. [2]Power Dispatching and Control Center, China Southern Power Grid, Guangzhou, China. [3]Shandong Shanda Electric Power Technology Co. LTD, Ji'nan, China.

Received: 20 December 2021 Accepted: 27 May 2022
Published online: 13 June 2022

**References**

1. Li, Z. X., Wan, J. L., Wang, P. F., Weng, H. L., & Li, Z. H. (2021). A novel fault section locating method based on distance matching degree in distribution network. *Protection and Control of Modern Power Systems, 6*(2), 253–263.
2. Xiao, Y., Ouyang, J. X., Xiong, X. F., Wang, Y. T., & Luo, Y. J. (2020). Fault protection method of single-phase break for distribution network considering the influence of neutral grounding modes. *Protection and Control of Modern Power Systems, 5*(2), 1–13.
3. Das, T., Roy, R., & Mandal, K. K. (2020). Impact of the penetration of distributed generation on optimal reactive power dispatch. *Protection and Control of Modern Power Systems, 5*(4), 63–89.
4. Liu, J. Y., Gao, H. J., Ma, Z., & Li, Y. X. (2015). Review and prospect of active distribution system planning. *Journal of Modern Power Systems and Clean Energy, 3*(4), 457–467.
5. Mohamed, A. (2021). High performance decoupled active and reactive power control for three-phase grid-tied inverters using model predictive control. *Protection and Control of Modern Power Systems, 6*(3), 311–329.
6. Coffele, F., Booth, C., & Dyśko, A. (2015). An adaptive overcurrent protection scheme for distribution networks. *IEEE Transactions on Power Delivery, 30*(2), 561–568.
7. Jia, K., Gu, C. J., Xuan, Z. W., Li, L., & Lin, Y. Q. (2018). Fault characteristics analysis and line protection design within a large-scale photovoltaic power plant. *IEEE Transactions on Smart Grid, 9*(5), 4099–4108.
8. Zhang, F., Mu, L., & Guo, W. (2019). An integrated wide-area protection scheme for active distribution networks based on fault components principle. *IEEE Transactions on Smart Grid, 10*(1), 392–402.
9. Sheng, S., Li, K. K., Chan, W. L., Zeng, X., Shi, D., & Duan, X. (2010). Adaptive agent-based wide-area current differential protection system. *IEEE Transactions on Industry Applications, 46*(5), 2111–2117.
10. Sortomme, E., Venkata, S. S., & Mitra, J. (2010). Microgrid protection using communication-sssisted digital relays. *IEEE Transactions on Power Delivery, 25*(4), 2789–2796.
11. Sortomme, E., Venkata, S. S., & Mitra, J. (2009). Microgrid protection using communication-assisted digital relays. *IEEE Transactions on Power Delivery, 25*(4), 2789–2796.
12. Yang, J., Lin, F., Zhou, C., Zou, G., Li, Y., & Qiao, S. (2019). Comparison protection method of current sequence components for feeder with distributed generation. *Power System Protection and Control, 47*(15), 116–123. in Chinese.
13. Jia, K., Yang, Z., Zhu, Z., Zheng, L., & Bi, T. (2019). Pilot protection based on current amplitude ratio for teed line in inverter-interfaced renewable energy power plants. *Electric Power Automation Equipment, 39*(12), 82–88. in Chinese.
14. Liu, S., Bi, T., Wang, X., Yang, G., Xue, A., & Yang, Q. (2016). Fault current characteristics of inverter interfaced renewable energy generators with asymmetrical fault ride-through capability. *Automation of Electric Power System, 40*(3), 66–73. in Chinese.
15. Gao, H., Li, J., & Xu, B. (2017). Principle and implementation of current differential protection in distribution networks with high penetration of DGs. *IEEE Transactions on Power Delivery, 32*(1), 565–574.
16. Zhou, C., Zou, G., Zang, L., & Du, X. (2022). Current differential protection for active distribution networks based on improved fault data self-synchronization method. *IEEE Transactions on Smart Grid, 13*(1), 166–178.
17. Zhou, C., Zou, G., Du, X., & Zang, L. (2022). Adaptive current differential protection for active distribution network considering time synchronization error. *International Journal of Electrical Power and Energy Systems, 140*, 1–12.
18. Si, X., Chen, Q., Gao, Z., Ma, J., Chen, M., & Wang, L. (2014). Protection scheme for active distribution system based on directions of current phase angle variation. *Automation of Electric Power System, 38*(11), 97–103. in Chinese.
19. Li, J., Gao, H., & Zhu, G. (2016). Inverse-time current differential protection in active distribution network considering characteristics of inverter-interfaced distributed generations. *Transactions of China Electrotechnical Society, 31*(17), 74–83. (in Chinese).
20. Chakeri, V., Seyedi, H., & Hagh, M. T. (2021). A new approach to transmission line pilot protection in the presence of inverter-interfaced distributed generators. *IEEE Systems Journal, 15*(4), 5383–5392.
21. Huang, W., Tai, N., Zheng, X., Fan, C., Yang, X., & Kirby, B. J. (2014). An impedance protection scheme for feeders of active distribution networks. *IEEE Transactions on Power Delivery, 29*(4), 1591–1602.
22. Chen, G., Liu, Y., & Yang, Q. (2020). Impedance differential protection for active distribution network. *IEEE Transactions on Power Delivery, 35*(1), 25–36.
23. Bolandi, T. G., Seyedi, H., Hashemi, S. M., & Nezhad, P. S. (2015). Impedance-differential protection: A new approach to transmission-line pilot protection. *IEEE Transactions on Power Delivery, 30*(6), 2510–2518.
24. Han, B., Li, H., Wang, G., Zeng, D., & Liang, Y. (2018). A virtual multi-terminal current differential protection scheme for distribution networks with inverter-interfaced distributed generators. *IEEE Transactions on Smart Grid, 9*(5), 5418–5431.
25. Shi, X., Zhang, H., Wei, C., Li, Z., & Chen, S. (2020). Fault modeling of IIDG considering inverter's detailed characteristics. *IEEE Access, 8*, 183401–183410.
26. Shuai, Z., Shen, C., Yin, X., Liu, X., & Shen, Z. J. (2018). Fault analysis of inverter-interfaced distributed generators with different control schemes. *IEEE Transactions on Power Delivery, 33*(3), 1223–1235.
27. Jena, S., & Bhalja, B. R. (2020). Sampled value-based bus zone protection scheme with dq-components. *IET Generation, Transmission and Distribution, 14*(20), 4520–4528.
28. He, L., Shuai, Z., Chu, X., Huang, W., Feng, Y., & Shen, Z. J. (2020). Waveform difference feature-based protection scheme for islanded microgrids. *IEEE Transactions on Smart Grid, 12*(3), 1939–1952.
29. Xu, M. (2017). Novel protection and control scheme and implementation technology for microgrid. M.S. thesis, Department of Electrical Engineering, Shandong University, Ji'nan, China, (in Chinese).